Journal of Hydrodynamics, Ser. B, 1(1997).
China Ocean Press, Beijing—Printed in China

A FINITE-DIFFERENCE RELAXATION SCHEME BASED ON BOTH MULTIGRID TECHNIQUES AND HOMOTOPY METHOD FOR 2D STEADY-STATE NAVIER-STOKES EQUATIONS

Liao Shi-jun, Zhu Ji-mao
Department of Naval Architecture & Ocean Engineering, Shanghai Jiao Tong University, Shanghai 200030, *P. R. China*

(Received Jan. 22, 1996)

ABSTRACT: In this paper, multigrid techniques together with homotopy method are applied to propose a kind of finite-difference relaxation scheme for 2D steady-state Navier-Stokes equations. The proposed numerical scheme can give convergent results for viscous flows with high Reynolds number. As an example, the results of shear-driven cavity flow with high Reynolds number up to 25000 on fine grid 257×257 are given.

KEY WORDS: 2D Navier-Stokes equations, multigrid techniques, homotopy method, shear-driven cavity flow

1. INTRODUCTION

The rapid development in computer science and industries gives us a chance to numerically solve complex engineering problems governed by differential or partial-differential equations. But up to now, it seems not easy to give numerical results of viscous flow governed by Navier-Stokes equations, especially for the flow in complex domain at high Reynolds number. For high Reynolds number, very fine computational grid is necessary so that a set of nonlinear algebraic equations with a large amount of unknowns is obtained after discretizing the Navier-Stokes equations on such a fine grid. There mainly exist two difficulties to solve this set of nonlinear algebraic equations. One is the convergence of the iterative schemes. Many iterative methods which are efficient at low Reynolds number diverge at high Reynolds number. The other is the rate of convergence which means the effectiveness of the calculations. The rate of convergence of many simple iterative methods is dependent upon the spacing step h of the computational grid. For example, the radius of spectrum of the Gauss-Seidel relaxation scheme and optimal SOR iteration are $1-O(h^2)$ and $1-O(h)$, respectively, so that, for very small h, the convergence is quite slow.

There exist some numerical techniques to accelerate the convergence of the relaxation schemes. One of them is multigrid method [2][3][4][6][14][16][19]. Multigrid method uses a series of computational grids and a simple relaxation scheme, as a smoother but not a solver on most grids except the coarsest one. The basic idea of multigrid method is to reduce the high-frequency components of the errors at current grid but to smooth out the low-frequency components of the errors at coarser grid. The radius of spectrum of multigrid method is generally independent upon the spacing step h of the finest computational grid so that its rate of convergence is generally still small even for very fine grid. The amount of calculations necessary for multigrid method is generally $O(N)$, where N is the number of all unknowns. Nowadays, multigrid method seems to be one of the most efficient acceleration techniques of solving complex partial-differential equations on very fine computational grid.

Generally, the convergence of most relaxation schemes, especially for non-linear pro-

© 1995-2004 Tsinghua Tongfang Optical Disc Co., Ltd. All rights reserved.

blems, is greatly dependent upon the selection of the initial approximations. Homotopy techniques [1][7][8][9][10][18] can overcome this disadvantage. Generally, for any suitable initial approximations, iterations based on homotopy techniques converge to one of the solutions. Owing to this reason, homotopy methods have been widely applied to give all zeros of nonlinear algebraic equations, to find the eigenvalues of problems, and so on. The author has used the basic ideas of homotopy method to propose a kind of high-order formulations of 2D steady-state Navier-Stokes equations which is suitable to boundary element method and can give results at high Reynolds number up to 10000, as described in [12] and [13].

In the present work, homotopy technique together with multigrid method are applied to give a finite-difference relaxation scheme of 2D Navier-Stokes equations. Our purpose is to develop a kind of efficient and convergent numerical scheme for viscous flow at high Reynolds number i. e. , a numerical scheme which converges at high Reynolds number but with the small amount of calculation $O(N)$.

In following sections, we at first describe the basic ideas of the proposed numerical scheme. Then, using the shear-driven flow in a square cavity as a simple example, we will show the effectiveness of the proposed method. The convergent results with high Reynolds number up to 25000 on very fine grid 257×257 are given.

2. MATHEMATICAL FORMULATIONS

Two-dimensional steady flow of an incompressible Newtonian fluid is formulated in terms of streamfunction (ψ) and the vorticity (ω) as follows:

$$\frac{1}{R_e}\nabla^2\omega = (u\omega)_x + (v\omega)_y \qquad (x,y)\in D \tag{1}$$

$$\nabla^2\psi + \omega = 0 \qquad (x,y)\in D \tag{2}$$

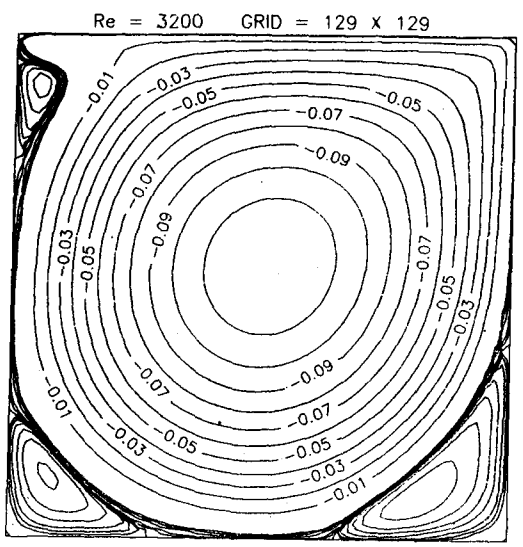

Fig. 1 Contour of streamfunction ψ in the case $R_e = 3200$

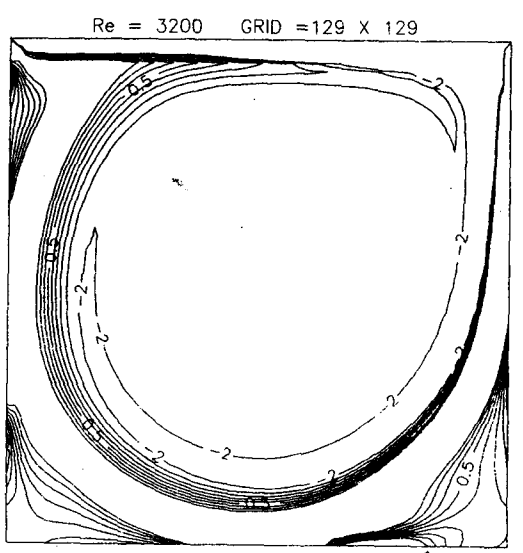

Fig. 2 Contour of vorticity ω in the case $R_e = 3200$

with boundary conditions:

© 1995-2004 Tsinghua Tongfang Optical Disc Co., Ltd. All rights reserved.

$$\psi = \psi_b \qquad \text{on } \partial D \tag{3}$$

$$\frac{\partial \psi}{\partial n} = (\frac{\partial \psi}{\partial n})_b \qquad \text{on } \partial D \tag{4}$$

The above equations are expressed in dimensionless form. $\mathrm{Re} = \rho v_0 L/\mu$ is the Reynolds number expressed in terms of a characteristic length L and a characteristic velocity v_0. The two independent co-ordinates x and y are also dimensionless, $u = \psi_y$ and $v = -\psi_x$ are two components of the velocity in x and y directions. D denotes the domain of the flow and ∂D denotes the corresponding boundary.

3. APPLICATIONS OF HOMOTOPY TECHNIQUES

Let p denote imbedding parameter. We construct two kinds of homotopy $\Omega(x,y;p) : D \times [0,1] \to R$ and $\Psi(x,y;p) : D \times [0,1] \to R$, which satisfy the governing equations

$$\frac{1}{\mathrm{R_e}}\nabla^2\Omega = p\{(U\Omega)_x + (V\Omega)_y\} + \frac{(1-p)}{\mathrm{R_e}}\nabla^2\omega_0 \qquad p \in [0,1],(x,y) \in D \tag{5}$$

$$\nabla^2\Psi + \Omega = (1-p)(\nabla^2\psi_0 + \omega_0) \qquad p \in [0,1],(x,y) \in D \tag{6}$$

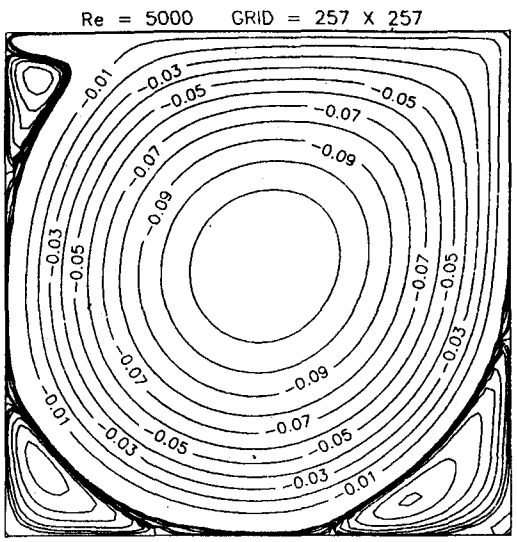

Fig. 3 Contour of streamfunction ψ in the case $R_e = 5000$

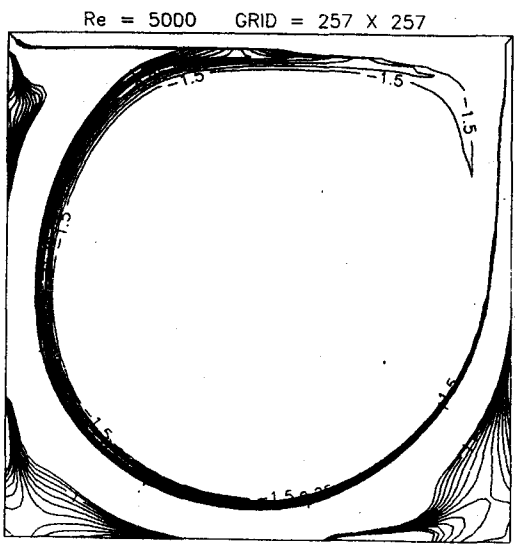

Fig. 4 Contour of vorticity ω in the case $R_e = 5000$

and the boundary conditions on ∂D :

$$\Psi = p\psi_b + (1-p)\psi_0 \qquad p \in [0,1],(x,y) \in \partial D \tag{7}$$

$$\frac{\partial \psi}{\partial n} = p(\frac{\partial \psi}{\partial n})_b + (1-p)\frac{\partial \psi_0}{\partial n} \qquad p \in [0,1],(x,y) \in \partial D \tag{8}$$

where $\psi_0(x,y)$ and $\omega_0(x,y)$ are free selected initial approximations of $\psi(x,y)$ and $\omega(x,y)$, respectively, and moreover $U = \partial\Psi/\partial y$, $V = -\partial\Psi/\partial x$. For simplicity, call Eqs. (5) (6) (7) (8) the zero-order deformation equations.

© 1995-2004 Tsinghua Tongfang Optical Disc Co., Ltd. All rights reserved.

Note that, in case $p = 1$, Eqs. (5) (6) (7) (8) are the same as Eqs. (1) (2) (3) (4), respectively. So, we obviously have

$$\omega(x,y) = \Omega(x,y;1) \tag{9}$$
$$\psi(x,y) = \Psi(x,y;1) \tag{10}$$

Clearly, there exist

$$\Omega(x,y;0) = \omega_0(x,y) \tag{11}$$
$$\Psi(x,y;0) = \psi_0(x,y) \tag{12}$$

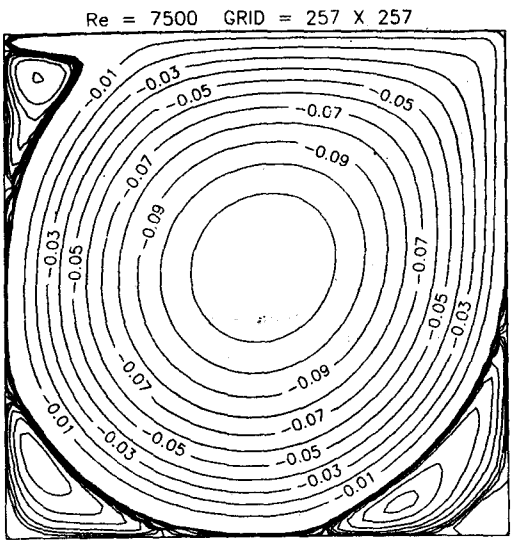

Fig. 5 Contour of streamfunction ψ in the case $R_e = 7500$

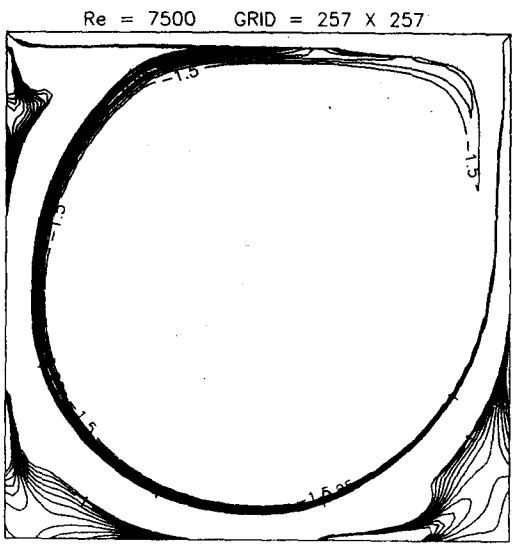

Fig. 6 Contour of vorticity ω in the case $R_e = 7500$

Thus, $\omega(x,y)$ and $\omega_0(x,y)$ are homotopic, so are $\psi(x,y)$ and $\psi_0(x,y)$, denoted respectively as

$$\Omega(x,y;p) : \omega(x,y) \simeq \omega_0(x,y) \tag{13}$$
$$\Psi(x,y;p) : \psi(x,y) \simeq \psi_0(x,y) \tag{14}$$

Let

$$\Omega^{[1]}(x,y;p) = \frac{\partial \Omega(x,y;p)}{\partial p} \tag{13}$$
$$\Psi^{[1]}(x,y;p) = \frac{\partial \Psi(x,y;p)}{\partial p} \tag{14}$$

denote the derivatives of $\Omega(x,y;p)$ and $\Psi(x,y;p)$ with respect to the imbedding parameter p, respectively. For simplicity, call them the first order deformation derivatives. Then, owing to expressions (9) (10) (11) (12), there exist

© 1995-2004 Tsinghua Tongfang Optical Disc Co., Ltd. All rights reserved.

$$\omega(x,y) = \omega_0(x,y) + \int_0^1 \Omega^{[1]}(x,y;p)\mathrm{d}p \tag{15}$$

$$\psi(x,y) = \psi_0(x,y) + \int_0^1 \Psi^{[1]}(x,y;p)\mathrm{d}p \tag{16}$$

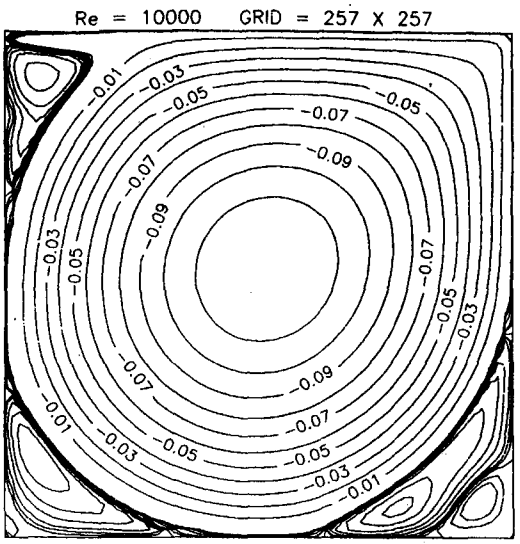

Fig. 7 Contour of streamfunction ψ in the case $R_e = 10000$

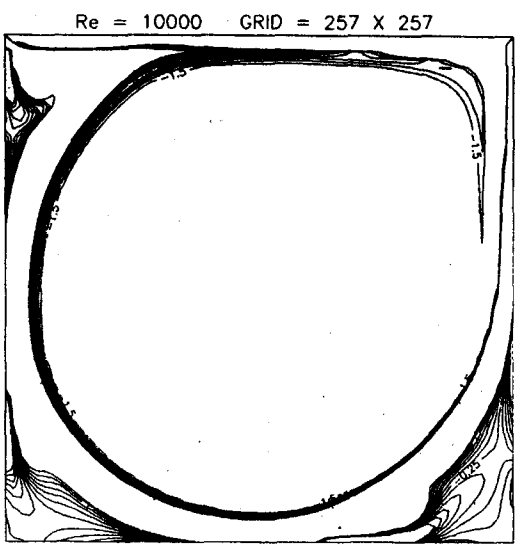

Fig. 8 Contour of vorticity ω in the case $R_e = 10000$

The governing equations of $\Omega^{[1]}(x,y;p)$ and $\Psi^{[1]}(x,y;p)$ can be obtained by simply differentiating Eqs. (5) (6) with respect to the imbedding parameter p, respectively, as follows

$$\frac{1}{\mathrm{R_e}}\nabla^2\Omega^{[1]} - p[(U\Omega^{[1]})_x + (V\Omega^{[1]})_y] - p[(U^{[1]}\Omega)_x + (V^{[1]}\Omega)_y] = \mathrm{R}_\omega(x,y;p)$$
$$p \in [0,1], (x,y) \in D \tag{17}$$

$$\nabla^2\Psi^{[1]} + \Omega^{[1]} = \mathrm{R}_\psi(x,y)$$
$$p \in [0,1], (x,y) \in D \tag{18}$$

where

$$\mathrm{R}_\omega(x,y;p) = -\{\frac{1}{\mathrm{R_e}}\nabla^2\omega_0 - [(U\Omega)_x + (V\Omega)_y]\} \tag{19}$$

$$\mathrm{R}_\psi(x,y) = -\{\nabla^2\psi_0 + \omega_0\} \tag{20}$$

and

$$U^{[1]}(x,y;p) = \frac{\partial\Psi^{[1]}(x,y;p)}{\partial y}$$

$$V^{[1]}(x,y;p) = -\frac{\partial\Psi^{[1]}(x,y;p)}{\partial x}$$

© 1995-2004 Tsinghua Tongfang Optical Disc Co., Ltd. All rights reserved.

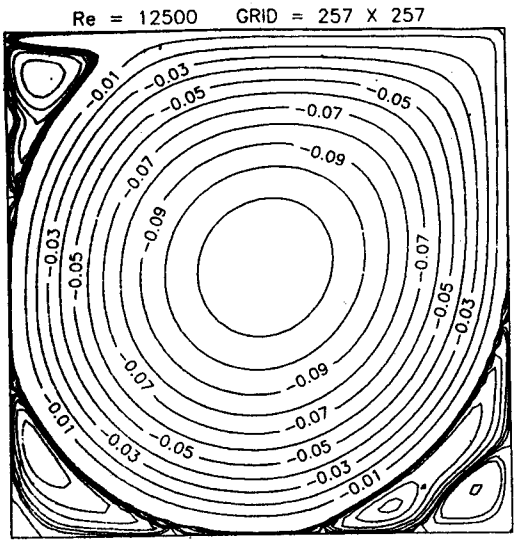

Fig. 9 Contour of streamfunction ψ in the case $R_e = 12500$

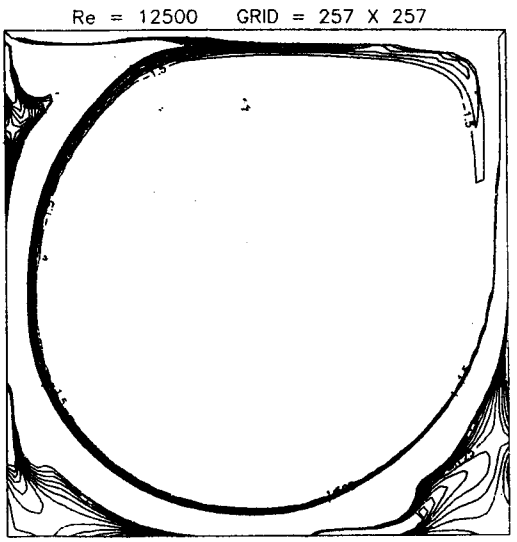

Fig. 10 Contour of vorticity ω in the case $R_e = 12500$

Similarly, differentiating Eqs. (7) and (8) with respect to p gives the corresponding boundary conditions

$$\Psi^{[1]}(x,y;p) = \psi_b - \psi_0 \qquad p \in [0,1], (x,y) \in \partial D \tag{21}$$

$$\frac{\partial \psi^{[1]}(x,y;p)}{\partial n} = (\frac{\partial \psi}{\partial n})_b - (\frac{\partial \psi_0}{\partial n}) \qquad p \in [0,1], (x,y) \in \partial D \tag{22}$$

Note that Eqs. (17) (18) (21) (22) are linear partial-differential ones about $\Omega^{[1]}(x, y;p)$ and $\Psi^{[1]}(x,y;p)$ for every fixed values of $p \in [0,1]$, which can be solved by many numerical methods. For simplicity, call Eqs. (17) (18) (21) (22) the first-order deformation equations.

Not that $R_\omega(x,y;p)$ is changing as p increases, because $\Omega(x,y;p)$, $\Psi(x,y;p)$, $U(x, y;p)$ and $V(x,y;p)$ are functions about the imbedding parameter p. Clearly, $R_\omega(x,y;0)$ and $R_\psi(x,y)$ denote the residuals of the Eqs. (1) and (2), respectively, for the free selected initial approximations $\omega_0(x,y)$ and $\psi_0(x,y)$. It should be emphasized that, in case $\omega_0(x, y)$, $\psi_0(x,y)$ are the solutions of the original Eqs. (1) (2) (3) (4), $R_\omega(x,y;p)$ and $R_\psi(x, y)$ are zero so that $\Omega(x,y;p)$, $\Psi(x,y;p)$ are equal to null in domain D for any $p \in [0,1]$. So, as p increases, the functions $\Omega(x,y;p)$ and $\Psi(x,y;p)$, governed by the zero-order deformation Eqs. (5) (6) (7) (8), are deformed in such a way that the errors given by the free selected initial approximations $\omega_0(x,y)$ and $\psi_0(x,y)$ will be reduced, and the directions of the deformation are governed by the first-order deformation Eqs. (17) (18) (21) (22). Our numerical tests show that, for any $0 \leqslant p_1 < p_2 \leqslant 1$, $\Omega(x,y;p_2)$, $\Psi(x,y;p_2)$ are always better approximations than $\Omega(x,y;p_1)$, $\Psi(x,y;p_1)$, respectively.

After $\Omega^{[1]}(x,y;p)$ and $\Psi^{[1]}(x,y;p)$ are obtained, $\Omega(x,y;p + \Delta p)$ and $\Psi(x,y;p + \Delta p)$ are given by Runge-Kutta's method.

4. APPLICATION OF MULTIGRID METHOD

© 1995-2004 Tsinghua Tongfang Optical Disc Co., Ltd. All rights reserved.

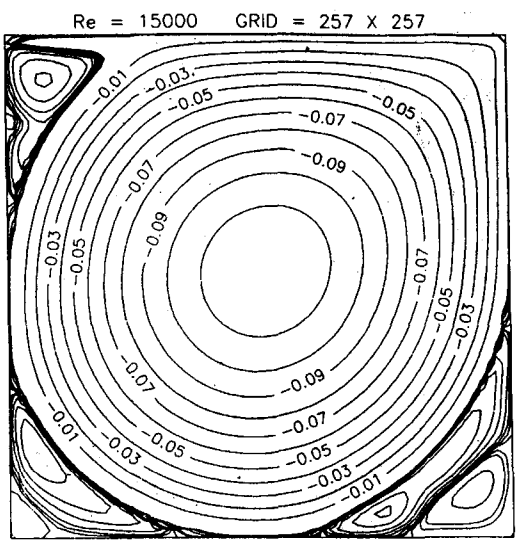

Fig. 11 Contour of streamfunction ψ in the case $R_e = 15000$

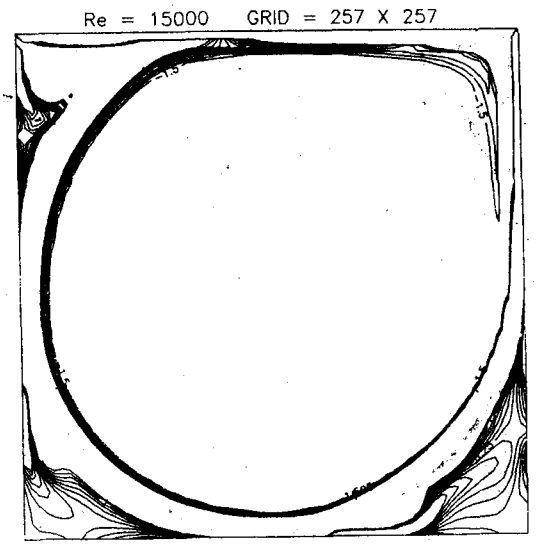

Fig. 12 Contour of vorticity ω in the case $R_e = 15000$

We solve the linear partial-differential Eqs. (17) (18) (21) (22) (the first-order deformation equations) by means of multigrid method. The multigrid method makes use of a series of computational grid G_k, $k = 0,1,2,\cdots,M$. Let h_k denote the step size on G_k and $h_{k+1} = h_k/2$ holds, so that as k increases, G_k becomes finer. The basic ideas of multigrid method are using simple iterative techniques as a smoother but not a solver to reduce the high-frequency components of the error on grid G_k and to smooth out the low-frequency components of the error on coarser grid G_{k-1}. For details, please see references [2][3][4][6][14][16][19].

Because the first-order deformation Eqs. (17) (18) (21) (22) are linear partial-differential ones, the Full Approximation Storage (FAG) Algorithm [2][3] isn't used here in order to reduce the amount of calculations. In this paper, we apply V-cycle multigrid scheme [14].

4.1 *Restriction and prolongation operators*

For transfer of functions w from fine to coarse grids (restriction) or from coarse to fine grids (prolongation), the corresponding operators should be selected. Similar as Wesseling [19], we use in this paper the 9-point restriction operator R_k^{k-1}:

$$(R_k^{k-1}w^k)_{i+1,j+1} = \frac{1}{4}w^k_{2i+1,2j+1} + \frac{1}{8}\{w^k_{2i+2,2j+1} + w^k_{2i+1,2j+2} + w^k_{2i,2j+1} + w^k_{2i+1,2j}\}$$
$$+ \frac{1}{16}\{w^k_{2i+2,2j+2} + w^k_{2i,2j+2} + w^k_{2i+2,2j} + w^k_{2i,2j}\} \tag{23}$$

and the 9-point prolongation operator P_{k-1}^k:

$$(P^k_{k-1}w^{k-1})_{2i+1,2j+1} = w^{k-1}_{i+1,j+1} \tag{24}$$
$$(P^k_{k-1}w^{k-1})_{2i+2,2j+1} = \frac{1}{2}\{w^{k-1}_{i+1,j+1} + w^{k-1}_{i+2,j+1}\} \tag{25}$$
$$(P^k_{k-1}w^{k-1})_{2i+1,2j+2} = \frac{1}{2}\{w^{k-1}_{i+1,j+1} + w^{k-1}_{i+1,j+2}\} \tag{26}$$

© 1995-2004 Tsinghua Tongfang Optical Disc Co., Ltd. All rights reserved.

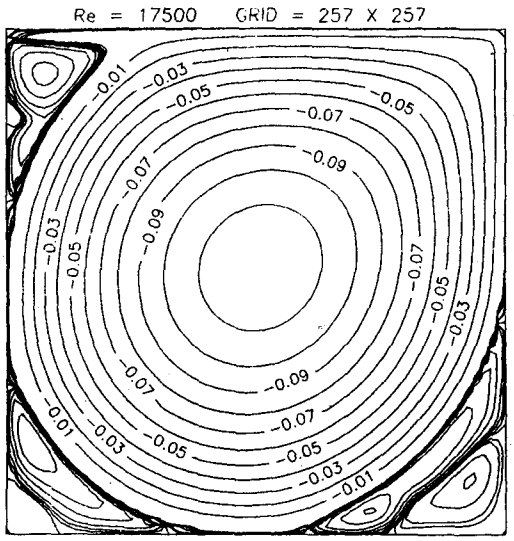

Fig. 13 Contour of streamfunction ψ in the case $R_e = 17500$

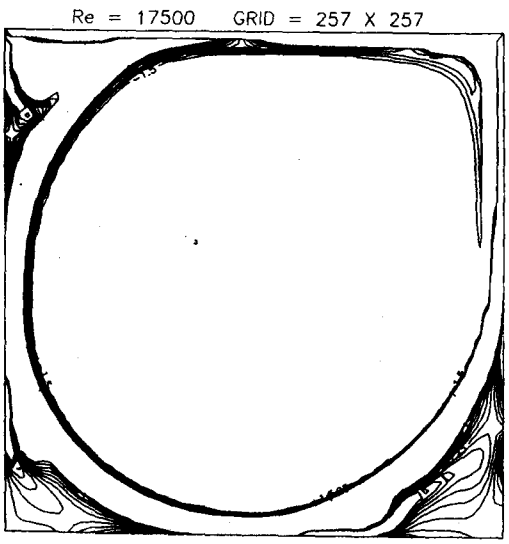

Fig. 14 Contour of vorticity ω in the case $R_e = 17500$

$$(P_{k-1}^{k} w^{k-1})_{2i+2,2j+2} = \frac{1}{4}\{w_{i+1,j+1}^{k-1} + w_{i+2,j+1}^{k-1} + w_{i+1,j+2}^{k-1} + w_{i+2,j+2}^{k-1}\} \tag{27}$$

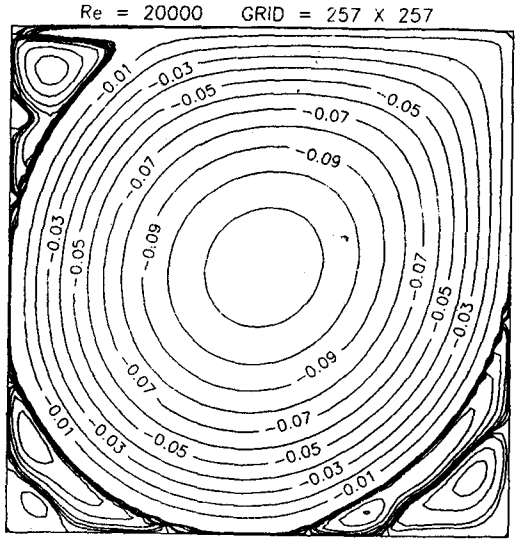

Fig. 15 Contour of streamfunction ψ in the case $R_e = 20000$

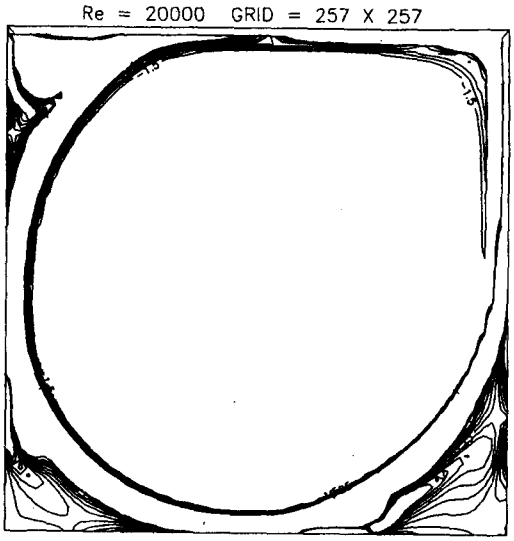

Fig. 16 Contour of vorticity ω in the case $R_e = 20000$

4.2 *Smoothing operator*

We use SOR (Successive Over Relaxation) method as the smoothing operator S^{v}, where v denotes the number of the iterations. Second-order accurate central finite-difference approximations are employed for all second-order derivatives in equations (17) and (18).

© 1995-2004 Tsinghua Tongfang Optical Disc Co., Ltd. All rights reserved.

The convective terms

$$(U\Omega^{[1]})_x + (V\Omega^{[1]})_y$$

are represented via a first-order accurate upwind difference scheme, but second-order accurate central finite-difference approximations are employed for all other first-order derivatives in Eqs. (17) and (18). On boundary ∂D, we use second-order accurate approximations [5]:

$$\nabla^2\Psi_j^{[1]} = \frac{1}{2h^2}\{8\Psi_{j-1}^{[1]} - \Psi_{j-2}^{[1]} - 7\Psi^{[1]}|_{\partial D} - 6\frac{\partial\Psi^{[1]}}{\partial n}|_{\partial D}h\} \tag{28}$$

Owing to (18), the values of $\Omega^{[1]}(x,y;p)$ on boundary ∂D are obtained as follows

$$\begin{aligned}\Omega_j^{[1]} &= R_\psi(x,y) - \nabla^2\Psi^{[1]}(x,y;p)|_{\partial D} \\ &= R_\psi(x,y) - \frac{1}{2h^2}\{8\Psi_{j-1}^{[1]} - \Psi_{j-2}^{[1]} - 7\Psi^{[1]}|_{\partial D} - 6\frac{\partial\Psi^{[1]}}{\partial n}|_{\partial D}h\}\end{aligned} \tag{29}$$

where $\Psi^{[1]}|_{\partial D}$ and $\frac{\partial\Psi^{[1]}}{\partial n}|_{\partial D}$ are given by Eqs. (21) and (22), respectively.

In this paper, we select 0.75 as the relaxation parameter for both governing Eqs. (17) (18) and the corresponding boundary conditions (21) (22) (29).

The value of υ for operator S^υ is different for different grid $G_k(k = 0,1,2,\cdots,M)$. The operator S^υ is used as a smoother on grid $G_k(1 \leqslant k \leqslant M)$ except on the coarsest grid G_o. In this paper, we set $\upsilon = 1$ for G_M and $\upsilon = 2$ for $G_k(0 < k < M)$. On grid G_o, operator S^υ is used as a solver, so υ should be large enough to make the iteration convergent.

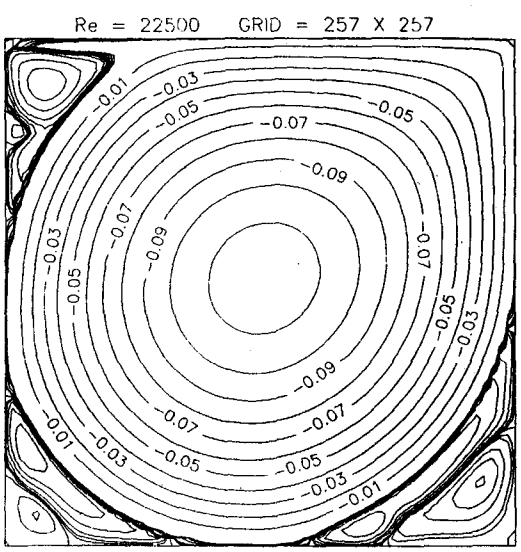

Fig. 17 Contour of streamfunction ψ in the case $R_e = 22500$

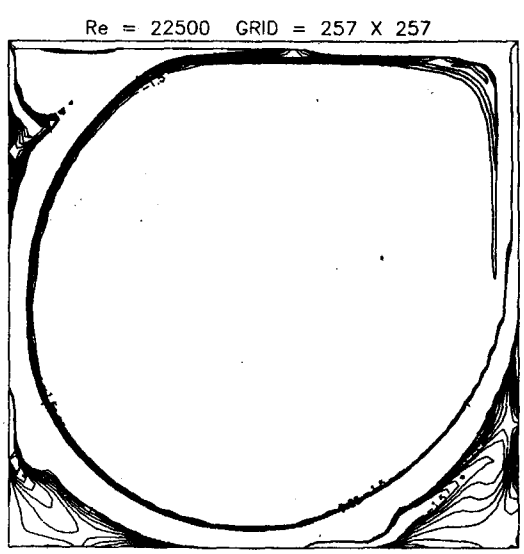

Fig. 18 Contour of vorticity ω in the case $R_e = 22500$

Convergence is defined to occur when the Euclid norm of the dynamic residuals $\mathbf{r} =$

© 1995-2004 Tsinghua Tongfang Optical Disc Co., Ltd. All rights reserved.

$\{r_l,\ l=1,2,\cdots,K\}$ of the governing equations and the corresponding boundary conditions is below a specified tolerance $\in$, i. e. ,

$$||\mathbf{r}|| = \sqrt{\frac{\sum_{l=1}^{l=K} r_l^2}{K}} < \in \tag{30}$$

where $K = N^2$ for grid $N \times N$.

There exist two convergence criterions, $\in_0$ and $\in_M$, respectively for the coarsest grid G_0 and the finest grid G_M . On grid G_0 , the convergence criterion is

$$||\mathbf{r}_0|| < \in_0 = \alpha^M ||\mathbf{r}_M|| \tag{31}$$

where $\alpha < 1$, and $||\mathbf{r}_0||$ and $||\mathbf{r}_M||$ are the Euclid norms of the residuals of the first-order deformation Eqs. (17) (18) (21) (22) on grid G_0 and G_M , respectively. In this paper, we set $\alpha = 1/2$ in most cases.

Let $||\mathbf{r}_M^0||$ denote the Euclid norm of the residuals of the original Eqs. (1) (2) (3) (4) on grid G_M . The convergence criterion for grid G_M is

$$||\mathbf{r}_M|| < \in_M = \frac{||\mathbf{r}_M^0||}{\beta} \tag{32}$$

where $\beta > 1$. We set $\beta = 10$ in this paper.

5. NUMERICAL SCHEME

The whole numerical scheme of the proposed method can be simply described as follows:

<1>Selecting $\omega_0(x,y)$ and $\psi_0(x,y)$ as the initial approximations for $p = 0$;

<2>Solving the first-order deformation Eqs. (17) (18) (21) (22)to obtain $\Omega^{[1]}(x, y;p)$ and $\Psi^{[1]}(x,y;p)$ by means of multigrid method;

<3>Obtaining $\Omega^{[1]}(x,y;p+\Delta p)$ and $\Psi^{[1]}(x,y;p+\Delta p)$ by means of Runge-Kutta's method;

<4>Setting $p = p + \Delta p$;

<5>Going to <2> if $p \leqslant 1$;

<6>Setting $\omega_0(x,y) = \Omega(x,y;1)$, $\psi_0(x,y) = \Psi(x,y;1)$ and going to <2> if the Euclid norm of the residuals of the original Eqs. (1) (2) (3) (4) is greater than a given tolerance ε_0 .

In the above-mentioned work, ε_0 is taken to be 10^{-3} for all cases. In case $R_e = 0$, select $\omega_0(x,y) = 0$, $\psi_0(x,y) = 0$ as the initial approximations. At high Reynolds-number, the convergent results obtained at lower R_e are used as the initial approximations.

6. NUMERICAL TEST: SHEAR-DRIVEN CAVITY FLOW

We use the shear-driven flow in a square cavity as a simple example to show the effectiveness of the relaxation scheme described above. The boundary conditions are

$u = 0$ at $x = 0$, $x = 1$, $y = 0$
$u = 1$ at $y = 1$
$v = 0$ at $x = 0$, $x = 1$, $y = 0$, $y = 1$

© 1995-2004 Tsinghua Tongfang Optical Disc Co., Ltd. All rights reserved.

The shear-driven flow in a square cavity has served over and over again as a model problem to test and evaluate numerical techniques. some results for high R_e have been obtained. Using a nonuniform 151×151 grid such that $\Delta x=\Delta y\simeq 1/400$ near the walls, Benjamin and Denny gave the results for $R_e=10000$. Using a uniform 121×121 grid together with a higher-order accurate upwind scheme, Agarwal obtained the results for $R_e=7500$. The results on a uniform 257×257 grid for R_e up to 10000 have been given by U. Ghia, K. N. Ghia and Shin [5]. In the current work, we will give the results on a uniform 257×257 grid for high R_e up to 25,000.

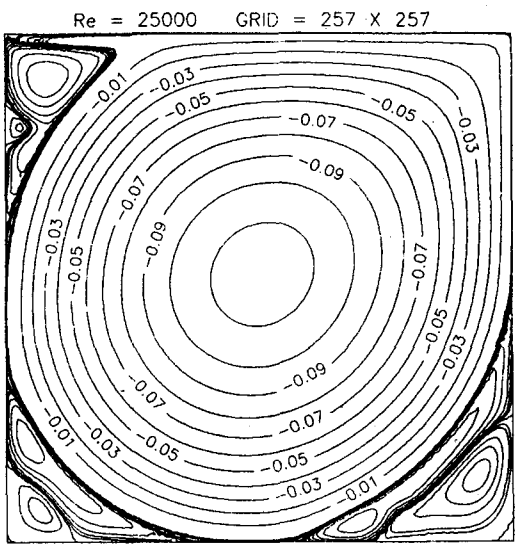

Fig. 19 Contour of streamfunction ψ in the case $R_e=25000$

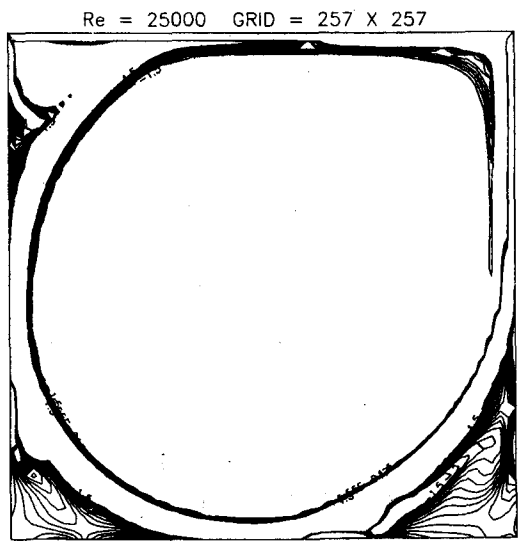

Fig. 20 Contour of vorticity ω in the case $R_e=25000$

The discretization is performed on a uniform mesh. The finest grid G_M is $N_0\times N_0$ with spacing step $h_M=1/(N_0-1)$. The coarse grids G_k are defined in such a way that $h_k=2h_{k+1}(k=0,1,2,\cdots,M-1)$. For $R_e\leqslant 3200$, $N_0=129$ gives fine enough results, as reported in [5]. But for $R_e>3200$, finer grid is necessary so that we set $N_0=257$.

At low R_e such as $R_e=0$ and $R_e=400$, $\Delta p=1$ is used. For $R_e=1000$ and $R_e=3200$, $\Delta p=1/2$ and $\Delta p=1/5$ are used, respectively. Generally, as R_e increases, Δp should be reduced. Our numerical tests show that the results $\Omega(x,y;p)$ and $\Psi(x,y;p)$ for any $p\in(0,1]$ are better approximations than $\omega_0(x,y)$ and $\psi_0(x,y)$, respectively, so that they can be used as better initial approximations to make the iteration scheme continuous.

We run our programme on PC (COMPAQ P4/50, 8M RAM). Owing to the limitations of the computer, let $M=4$ for low R_e. As R_e increases, the coarsest grid G_0 should be fine enough, as mentioned in [5]. So, let $M=2$ in case $R_e>15000$. About 10 minites are needed to obtain the result for R_e on 129×129 grid. But it needs about 23 hours by means of our PC to obtain the convergent results at $R_e=25000$ on 257×257 grid, including writing the results to hard disk at every iterations.

The contours of streamfunction ψ and vorticity ω are shown in Figs. 1—20, respectively. The values used for streamline contours are the same so that we can observe the changes of the streamline contours. The small values of the streamline contours which are not expressed in the figures are as follows:

© 1995-2004 Tsinghua Tongfang Optical Disc Co., Ltd. All rights reserved.

-7.0×10^{-4}, 2.5×10^{-5}, 1.0×10^{-3}
-5.0×10^{-4}, 5.0×10^{-5}, 2.0×10^{-3}
-3.0×10^{-4}, 1.0×10^{-4}, 3.0×10^{-3}
-1.0×10^{-4}, 2.5×10^{-4}, 4.0×10^{-3}
-5.0×10^{-5}, 5.0×10^{-4},

The velocity distribution of u at $x = 0.5$ and v at $y = 0.5$ for $R_e = 400$, 1000, 5000, 25000 are shown in Figs. 21 and 22, respectively.

For $R_e \leqslant 10000$, our results agree well with those reported in [5]. We are interested in the results for high R_e greater than 10000. As R_e increases ($R_e > 10000$), a new secondary vortex in the top left cornor of the cavity and also a new secondary vortex in the bottom left cornor appear and enlarge, shown as Figs. 9, 11, 13, 15, 17 and 19. In the bottom right cornor of the cavity, the second secondary vortex enlarges, which compresses the first secondary vortex, while the third secondary vortex appears and enlarges.

Obviously, there exist the thin wall boundary layers which is thinning as R_e increases, shown as Figs. 21 and 22. At high Reynolds number, the velocity profiles are near-linear in the central core of the cavity and exhibit a kink near $y = 1$ for the velocity u at $x = 0.5$ and also a kink near $x = 1$ for the velocity v at $y = 0.5$, shown as Figs. 21 and 22, respectively. Such behaviors have been reported by many previous researchers.

The results about the center of the primary vortex, the values of vorticity and stream-function there, denoted respectively as $\omega_{v,c}$ and $\psi_{v,c}$, are given in Table 1, together with the comparisons with those reported by U. Ghis, K. N. Ghia & C. T. Shin [5]. For $R_e = 10000$, $|\omega_{v,c}|$ is equal to 1.8728, close to the infinite-R_e value of 1.886 that is obtained by applying vortex together with the boundary layer corrections. But, as R_e increases, $|\omega_{v,c}|$ reduces and does not approach 1.886. For $R_e = 25000$, $|\omega_{v,c}|$ is equal to 1.7913. This is mainly because the values of ω and ψ at the center of primary vortex are sensitive to mesh size, as mentioned in [5]. Our calculations give an approach of the center of the primary vortex to (0.5078, 0.5273).

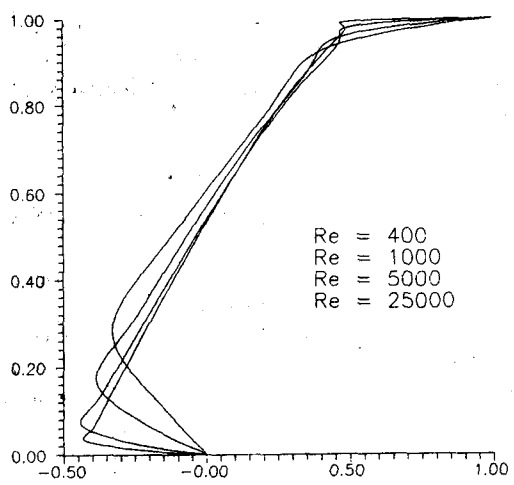

Fig. 21 Velocity distribution of u at $x = 0.5$

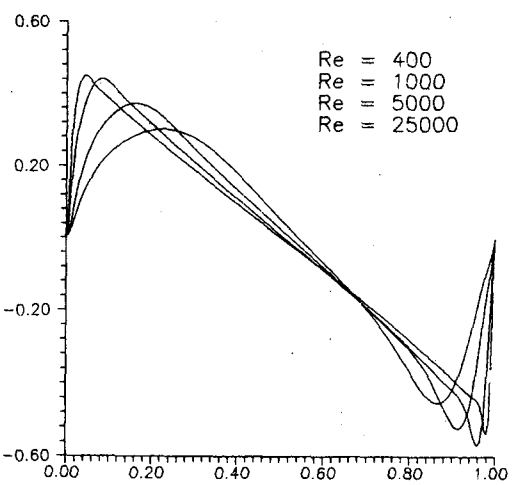

Fig. 22 Velocity distribution of v at $y = 0.5$

© 1995-2004 Tsinghua Tongfang Optical Disc Co., Ltd. All rights reserved.

Table. 1 Comparisons of the results about primary vortex with those given by Ghia, Ghia & Shin

R_e	present results			results reported in [5]		
	ψ_{max}	$\lvert\omega_{v,c}\rvert$	$(x,y)_{v,c}$	ψ_{max}	$\lvert\omega_{v,c}\rvert$	$(x,y)_{v,c}$
400	−0.11365	2.2881	(0.5547,0.6094)	−0.11391	2.2947	(0.5547,0.6055)
1000	−0.11802	2.0519	(0.5313,0.5625)	−0.11793	2.0497	(0.5313,0.5625)
3200	−0.11866	1.9109	(0.5156,0.5391)	−0.12038	1.9886	(0.5165,0.5469)
5000	−0.12080	1.9180	(0.5156,0.5352)	−0.11897	1.8602	(0.5117,0.5352)
7500	−0.12016	1.8923	(0.5117,0.5313)	−0.11998	1.8799	(0.5117,0.5322)
10000	−0.11938	1.8728	(0.5117,0.5313)	−0.11973	1.8808	(0.5117,0.5333)
12500	−0.11857	1.8562	(0.5117,0.5313)	/	/	/
15000	−0.11776	1.8415	(0.5117,0.5273)	/	/	/
17500	−0.11696	1.8278	(0.5078,0.5273)	/	/	/
20000	−0.11617	1.8151	(0.5078,0.5273)	/	/	/
22500	−0.11537	1.8024	(0.5078,0.5273)	/	/	/
25000	−0.11462	1.7913	(0.5078,0.5273)	/	/	/

7 CONCLUSIONS

In the present work, we apply multigrid techniques together with homotopy method to propose a kind of finite-difference relaxation scheme for 2D steady-state Navier-Stokes equations. The proposed numerical scheme has the advantages of the two methods, i. e., the good property of convergence of homotopy method and the calculation effectiveness of the multigrid techniques. As a test example, the viscous shear-driven flow in a square cavity is considered and the results for R_e up to 25000 on the fine 257×257 computational grid have been obtained. Thus, the proposed numerical scheme can be used to solve effectively 2D steady viscous flows for very high Reynolds number.

REFERENCES

1. Albrecht Duld, 1972: Lectures on Algebraic Topology, Springer-Verlag, Berlin Heidelberg New York.
2. A. Brandt, 1973: Multi-Level Adaptive Technique (MLAT) for Fast Numerical Solution to Boundary Value Problems, Notes in Physics, Vol. 18, pp. 82−89, Springer-verlage Berlin.
3. A. Brandt, 1977: Multi-Level Adaptive Solutions to Boundary-Values Problems, Mathematics of Computation, Vol. 31, 138, pp. 333−390.
4. R. E. Bank and C. C. Dongles, 1985: Sharp Estimates for Multigrid Rates of Convergence with General Smoothing and Acceleration, SIAM J. Numer. Anal., 22.
5. U. Ghia, K. N. Ghia and C. T. Shin, 1982: High-Resolutions for Incompressible Flow Using the Navier-Stokes Equations and a Multigrid Method, Journal of Computational Physics, 48, 387−411.
6. D. Kamouitz and S. V. parter, 1985: A Study of Some Multigrid Ideas, Applied Math. and Compu., 17.
7. Kojima, M., Nishino, H. & Arima, N., 1979: A PL Homotopy for Finding All the Roots of a Polynomial, Math. Prog., 16, pp. 37−62.
8. Li, T. Y., Mallet-Paret, J. & Yorke, J. A., 1985: Regularity Results for Real Analytic Homo-

© 1995-2004 Tsinghua Tongfang Optical Disc Co., Ltd. All rights reserved.

topies, Numer. Math., 46, pp 43—50.
9. Li, T. Y. & Sauer, T., 1987: Regularity Results for Solving Systems of Polynomials by Homotopy Method, Numer. Math., 50, pp 283—310.
10. Li, T. Y. & Sauer, T., 1987: Homotopy Methods for Generalized Eigenvalue Problems, Lin. Alg. Appl., 91, pp 65—74.
11. Liao, S. J., 1995: A Kind of Approximate Solution Technique Which Does Not Depend upon Small Parameters: a Special Example; Int. J. Nonlinear Mechanics, Vol. 30, No. 3, pp. 371—380.
12. Liao, S. J. & Zhu, J. M., 1996: A Short Note on the High-Order Streamfunction-Vorticity BEM formulations of 2D Steady-State Navier-Stokes Equation, Int. J. Numer. Methods Fluids, Vol. 22, pp. 1—9.
13. S. J. Liao, 1992: Higher-Order Streamfunction-Vorticity Formulation of 2D Steady-State Navier-Stokes Equations, Int. J. Numer. Methods Fluids, Vol. 15, pp. 595—612.
14. S. V. Parter, 1985: A Note on Convergence of the Multigrid V-Cycle, Applied Math. & Comput., 17.
15. Georges Papy, 1970: Topologie als Grundlage des Analysis-Unterrichts, Van-denholck & Ruprecht in Gottingen.
16. S. Schaffer, 1984: Higher-Order multigrid methods, Comput., 43.
17. Stoer Bulirsch, 1978: Einfuhrung in die Numerische Mathematik I ,springer-Verlag, Berlin.
18. Z. K. Wang & T. A. Kao, 1991: An Introduction to Homotopy Methods, Chongqing Publishing House, CHONGQING.
19. P. Wesseling, 1980: Theoretical and practical Aspects of a Multi Grid Method, Report NA-37, Delft University of technology, The Netherland.

© 1995-2004 Tsinghua Tongfang Optical Disc Co., Ltd. All rights reserved.